Algorithms for the Detection of First Bottom Returns and Objects in the Water Column in Sidescan Sonar Images

Conference Paper · March 2018

DOI: 10.1109/OCEANSE.2017.8084587

CITATIONS
0

READS
103

9 authors, including:

Baran Çürüklü
Mälardalen University
43 PUBLICATIONS **126** CITATIONS
SEE PROFILE

Xin Yuan
Universidad Politécnica de Madrid
4 PUBLICATIONS **15** CITATIONS
SEE PROFILE

Joaquim Bastos
Institute of Telecommunications
48 PUBLICATIONS **133** CITATIONS
SEE PROFILE

Algorithms for the Detection of First Bottom Returns and Objects in the Water Column in Sidescan Sonar Images

Mohammed Al-Rawi[1], Fredrik Elmgren[2], Mirgita Frasheri[3], Baran Cürüklü[3], Xin Yuan[4], José-Fernán Martínez[4], Joaquim Bastos[5], Jonathan Rodriguez[1], Marc Pinto[6]

[1] Departamento de Eletrónica, Telecomunicações e Informática (DETI), Universidade de Aveiro, Aveiro 3810-193, Portugal
al-rawi@ua.pt, jonathan@ua.pt

[2] DeepVision AB, Linköping, Sweden
fredrik@deepvision.se

[3] Mälardalen University, Box 883, 721 23 Västerås, Sweden
mirgita.frasheri@mdh.se, baran.curuklu@mdh.se

[4] Research Center on Software Technologies and Multimedia Systems for Sustainability (CITSEM), Universidad Politecnica de Madrid, Spain
xin.yuan@upm.es, jf.martinez@upm.es

[5] Instituto de Telecomunicações - Pólo de Aveiro, Aveiro 3810-193, Portugal
jbastos@av.it.pt

[6] ECA Robotics, 262 rue des frères Lumière, 83130 La Garde, France
mpi@eca.fr

Abstract— **Underwater imaging has become an active research area in recent years as an effect of increased interest in underwater environments and is getting potential impact on the world economy, in what is called blue growth. Since sound propagates larger distances than electromagnetic waves underwater, sonar is typically used for underwater imaging. One interesting sonar image setting is comprised of using two parts (left and right) and is usually referred to as sidescan sonar. The image resulted from sidescan sonars, which is called waterfall image, usually has to distinctive parts, the water column and the image seabed. Therefore, the edge separating these two parts, which is called the first bottom return, is the real distance between the sonar and the seabed bottom (which is equivalent to sensor primary altitude). The sensory primary altitude can be measured if the imaging sonar is complemented by interferometric sonar, however, simple sonar systems have no way to measure the first bottom returns other than signal processing techniques. In this work, we propose two methods to detect the first bottom returns; the first is based on smoothing cubic spline regression and the second is based on a moving average filter to detect signal variations. The results of both methods are compared to the sensor primary altitude and have been successful in 22 images out of 25.**

Keywords—edge detection; cubic smoothing spline; moving average filter; autonomous underwater vehicles

I. INTRODUCTION

One of the major problems related to underwater sonar imaging is the detection of the water-column, also known as the gap or the nadir area [1]. Usually, the water column bears trivial information compared to the seabed. The nadir area is usually generated in sidescan sonar images when the sound signal travels in the water layers until it reaches the seabed. Thus, the seabed echoes are the ones that are received after that the signal has passed the whole water column. Detecting these "first seabed bottom returns" is vital in the processing of sidescan sonar images [2, 3] when the sensor primary altitude is not available. First bottom returns are essential to several underwater sidescan images, for example, applying various correction filters to the across-track signals, speed correction, ground-range correction, etc. In a perfect scenario, however, the nadir edge should be a straight line, which is not the case in reality due to the disrupted underwater vehicle motion. The variations in the nadir area depend on several factors, e.g. the distance from the sonar head to the seabed, the movement direction of the vehicle carrying the sonar, and underwater currents [4, 5, 6]. Few models have been proposed to detect the bottom first returns [7, 8]. These models face serious challenges that may deteriorate the correct detection of the first bottom returns, e.g., due to echoes from various objects floating above the seabed.

Bottom tracking searches for the first strong echo of each scanline, and then links those for all pings as the sea bottom line in waterfall image. The sea bottom line is the boundary of the water column image and the seabed image. Currently, bottom tracking mainly adopts the threshold method. In [7], the author assumes proper compensation for transmission losses due to

spreading and absorption of acoustic energy in the water column, a threshold of 10 dB is chosen to detect echoes in the water column above and close to the bottom, with minimal masking caused by bottom echoes appearing in the sidelobes of other beams across the swath. A comprehensive tracking method has been proposed in [8], which combines the last peak method and the repair method of side scan sonar image abnormal bottom-tracking. Comparison results illustrate that their proposed method achieves higher accuracy of first returns detection relative to the traditional threshold method and the last peak method.

II. Methods

Autonomous Underwater Vehicles (AUVs) have been used to image the seabed using sidescan sonar(s), ECA's A9 AUV is shown in Fig. 1. The missions have been performed in Las Palmas de Gran Canaria (Spain) and have been planned to cover a large area resulting in 25 seabed images. The images have been recorded with a Klein 3500 sidescan sonar. The imaging data has been collected as part of the SWARMs project (Smart and Networking Underwater Robots in Cooperation Meshes; http://www.swarms.eu/). Accurate detection of the bottom first returns is usually part of several other tasks that are mainly related to process the seabed maps and to perform various functions on them, e.g., registration, matching, and fusion.

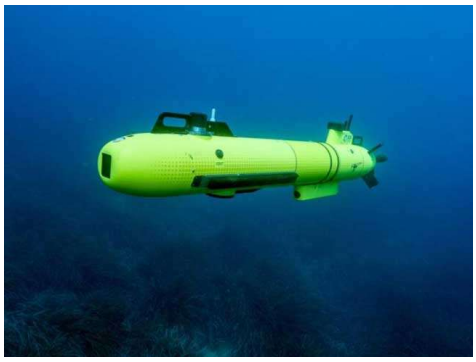

Fig. 1. ECA's A9 autonomous underwater vehicle that has been used in the missions.

The objective of this work is proposing methods to detect the first bottom returns in sidescan sonar images. To overcome the weaknesses found in previous approaches, we propose to use a smoothing cubic spline fitting method to detect the (hypothetical/approximate) center of the nadir area, as shown in Fig. 2. The parameters of the spline fitting model are estimated from each across-track samples. We found that applying the cubic spline regression on the $\log(x)$ of the signal gives improved fitting to the signals. Then, starting from the center of the nadir gap, the second phase of the algorithm detects the rise in the signal, compared to a chosen threshold value, hence finding the first return. This method is performed to each across-track signal.

Another algorithm that we propose to detect the first seabed returns is based on using a short-window average filter that is applied to each across-track signal. The hypothesis in this case is that the average of the signal in the middle of nadir area is lower than the first returns. After using the filter, the difference between each two consecutive points is calculated and the first return is detected when the difference is higher than a predefined threshold value. In this work, we used a filtering window of size 50 points, a signal obtained using the moving average filter is shown in Fig. 3.

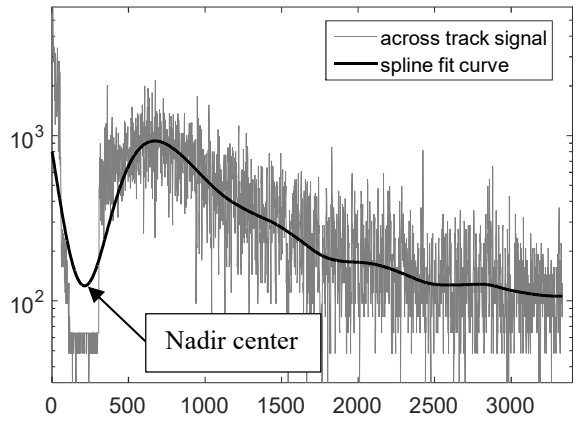

Fig. 2. Using cubic spline fitting to detect the center of the nadir gap. The black arrow marks the center of the nadir gap. Nadir center here is at location 213 and the first return is detected at location 307.

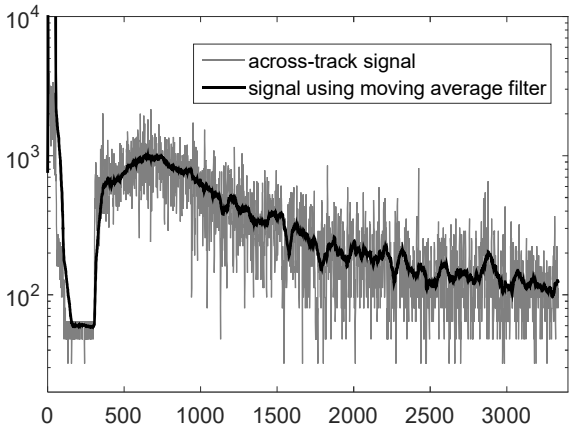

Fig. 3. Using the moving average filter on the same signal shown in Fig. 2. The first bottom return has been detected at location 306.

III. Experimental Results

Sidescan sonars have been used to capture the seabed in several locations in Las Palms de Gran Canaria. These sonars have been mounted/integrated in autonomous underwater vehicles (AUVs), one of which is shown in Fig. 1. To prepare the ground-truth values, the first returns have been manually detected by one of the authors of this article, depicted in Fig. 4. The first returns have been successfully detected by each of the two methods proposed in this work, one is shown in Fig. 9 after overlaying it over the image.

Detecting objects in the water column is necessary to eliminate the backscatter reflected from the object, which can be detected falsely as first return(s). An object in the water column, e.g., the one shown in Fig. 5 and Fig. 6, will spike high

somewhere in the along-track first returns as shown in Fig. 7 and Fig. 8. After detecting the first returns, objects in the water column can be removed by applying a median filter, or other highly dedicated filters, on the along-tack first returns.

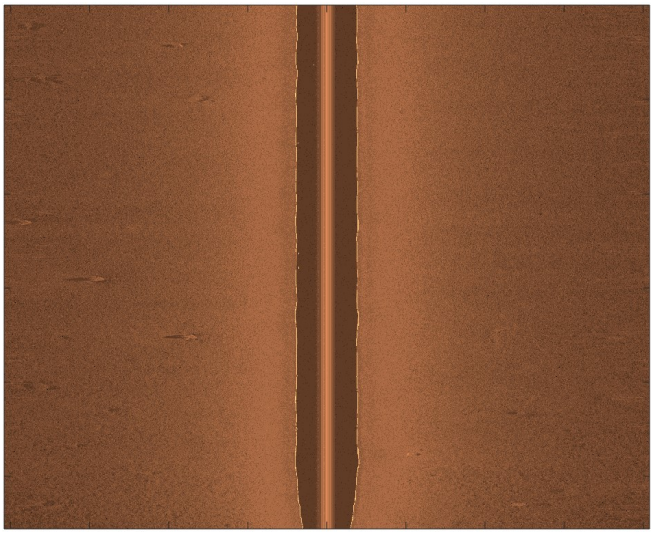

Fig. 4. The first returns (marked with yellow) that has been manually detected by one of the authors of this work.

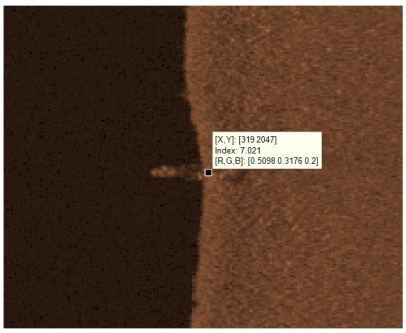

Fig. 5. Zoom at a region in the sonar image showing an object in the water column near the 2047th ping.

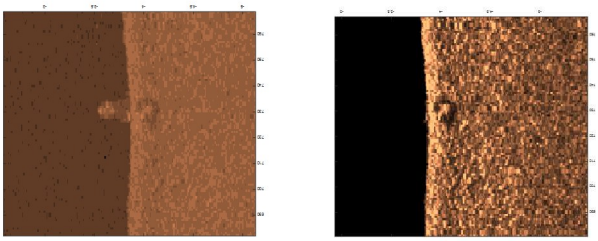

Fig. 6. A closer look, the log transformed image, on a region in the original image and the object is obvious in the water column (left), and the same area shown (right) but with the image being normalized and the object in the water-column removed. The shadow of the object is clear on the seafbed, which is the dark spot/ring close to the center of the image.

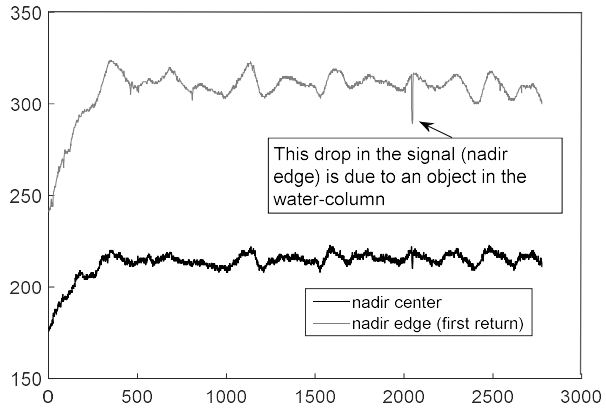

Fig. 7. Detecting objects in the water column.

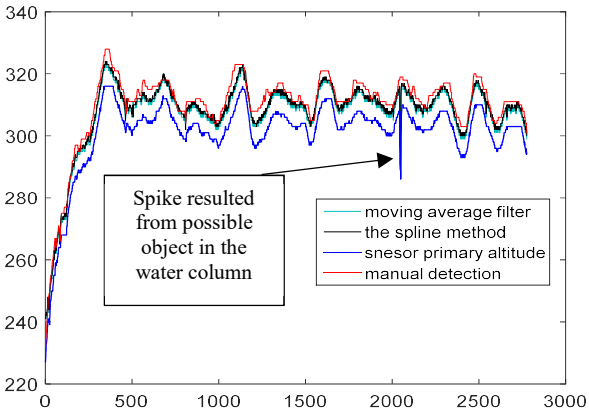

Fig. 8. First returns extracted from one image in this work. The x-axis denotes the location of the along-track ping and the y-axis denotes the values of the first returns. (Sensor primary altitude has been shifted 5 points below for clarity purpose)

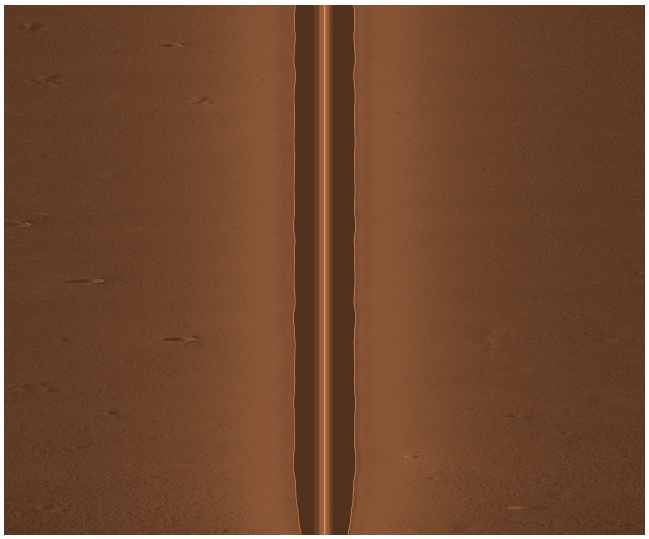

Fig. 9. The same image shown in Fig. 4 with the first returns, which are detected using the spline method, marked with yellow.

For this specific image demonstrated in Fig. 2, we performed cross-correlation analysis and the correlation coefficient between the used method and the sensor primary altitude; thus, correlation coefficients of the moving average filter, the spline method, and the manual method where 0.99, 0.99, and 0.89, respectively ($p<<0.05$; for all cases).

For an overall look on the proposed algorithms, we also performed cross correlation analysis, for all the 25 seabed images, between the sensor primary altitude and each of the two proposed algorithms, and for each of the left and the right scans. From the results depicted in Fig. 11, one can be seen that the detection of the first returns was not close to the sensor primary altitude in three images out of 25. By inspecting one of images that showed weaker first return detection, the right scan of image 5 from mission #2, we noticed a few objects in the water column that gone undetected. We compare the first returns of the left and the right scans and the peaks that resulted from water-column's objects can be seen clearly, as demonstrated in Fig. 12 and Fig. 13. Thus, more delicate object removal algorithm is used by treating the spike(s) in the along-track first returns as outliers [9]. The algorithms proposed in this work have been successful and they seem to overcome the manual marking of the first returns, as the latter is extremely hard task and could be subject to human error.

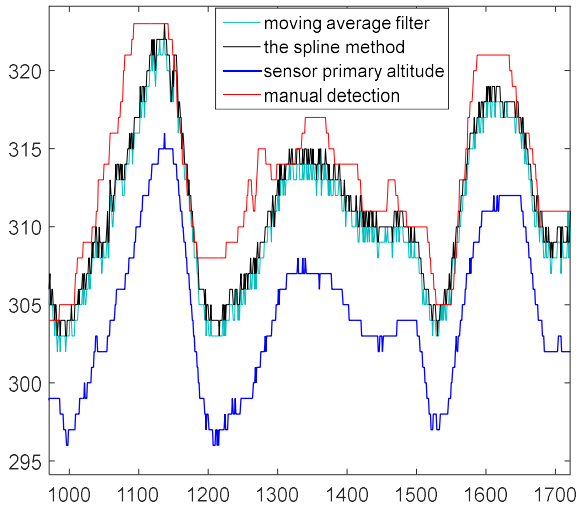

Fig. 10. Zooming part of the graph shown in Fig. 8. The x-axis denotes the location of the along-track ping and the y-axis denotes the values of the first returns. (Sensor primary altitude has been shifted 5 points below for clarity purpose)

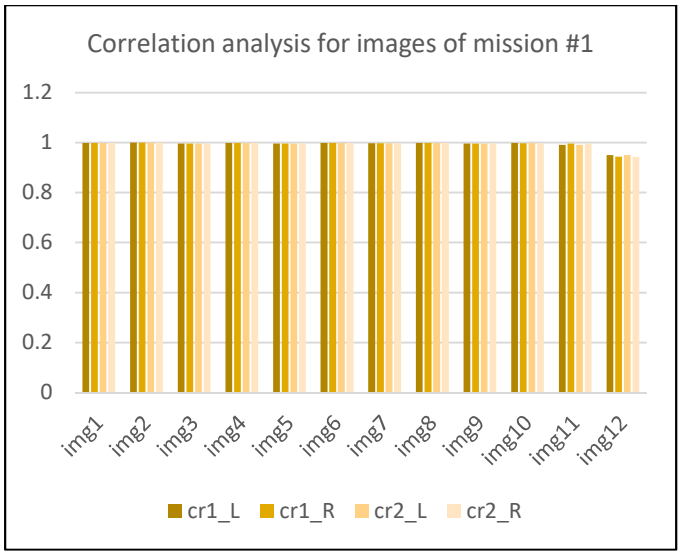

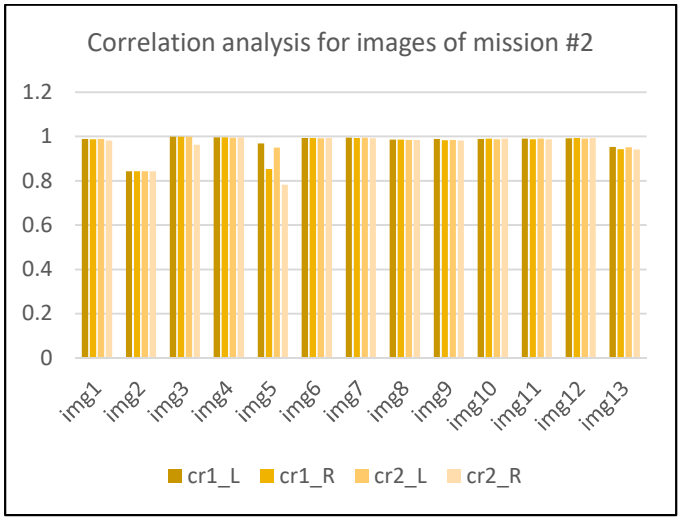

Fig. 11. Correlation analysis between the detected first bottom returns (using methods 1 and 2) and the measured sensor primary altitude. The correlation has been done for the left scan and then for the right scan. For example, cr1_L is the correlation between first bottom returns of the left scan using method 1 (the cubic spline) and the sensor primary altitued.

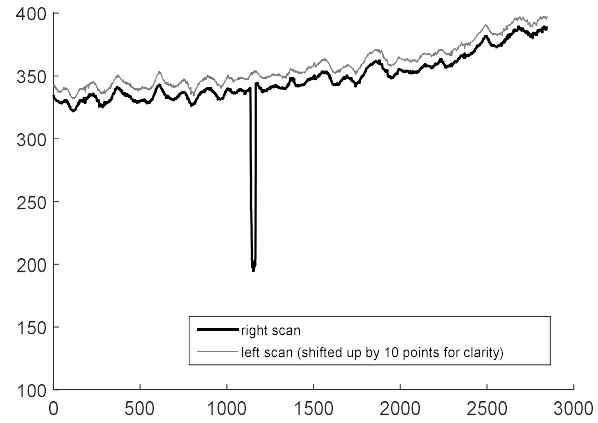

Fig. 12. First returns of image 2 in mission#2, showing differences (the spiked region) between left and right scan due to objects in the water column close to the right scan. The spike appreaed at samples 1136 to 1366. The left-scan first returns have been shifted by 10 points for clarity purpose.

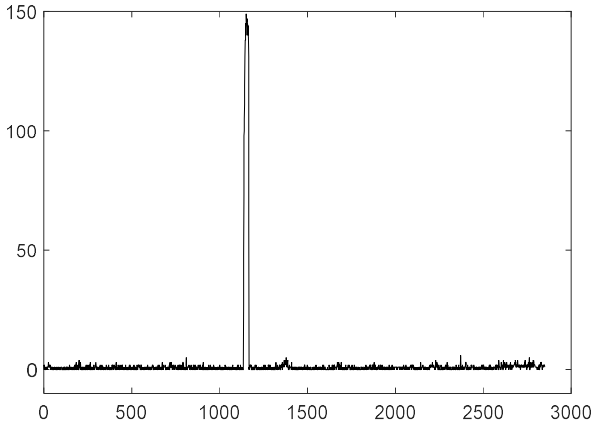

Fig. 13. The high peak resulted from the absolute differenc between the detected left and right first returns is used to correct the right scan. The cubic spline method, although was slower, perfored slightly better than the moving average filter method.

CONCLUSIONS

The proposed algorithms have been successful in detecting the first bottom returns. In addition to the simple methods we introduced to handle objects in the water-column, there is still work to be done for improving complicated scenarios, for example, two similar objects appearing in the water-column one closer to the left scan and the other is related to the right scan. As the algorithms have a few thresholding parameters, an important approach to be considered in future works is to make the methods compatible with different sidescan sonar devices.

ACKNOWLEDGMENT.

The research leading to the presented results has been undertaken within the SWARMs European project (Smart and Networking Underwater Robots in Cooperation Meshes), under Grant Agreement n. 662107-SWARMs-ECSEL-2014-1, which is partially supported by the ECSEL JU and the Fundação para a Ciência e a Tecnologia (ECSEL/0002/2014 and ECSEL/0003/2014). SWARMs project (http://www.swarms.eu/) aims at making autonomous underwater vehicles (AUVs) and remotely operated vehicles (ROVs) further accessible and useful for autonomous maritime operations.

REFERENCES

[1] R. P. Hodges, Underwater Acoustics: Analysis, Design and Performance of Sonar: Wiley, 2010.

[2] A. Burguera, and G. Oliver, "High-Resolution Underwater Mapping Using Side-Scan Sonar," Plos One, vol. 11, no. 1, Jan, 2016.

[3] A. Nait-Chabane, B. Zerr, and G. Le Chenadec, "Range-independent segmentation of sidescan sonar images," Traitement Du Signal, vol. 30, no. 3-5, pp. 119-148, May-Oct, 2013.

[4] Y.-C. Chang, S.-K. Hsu, and C.-H. Tsai, "Sidescan Sonar Image Processing: Correcting Brightness Variation and Patching Gaps," Journal of Marine Science and Technology-Taiwan, vol. 18, no. 6, pp. 785-789, Dec, 2010.

[5] C. G. Capus, A. C. Banks, E. Coiras, I. T. Ruiz, C. J. Smith, and Y. R. Petillot, "Data correction for visualisation and classification of sidescan SONAR imagery," IET Radar Sonar and Navigation, vol. 2, no. 3, pp. 155-169, Jun, 2008.

[6] MS Al-Rawi, Adrián Galdrán, Xin Yuan, Martina Eckert, José-Fernán Martínez, Fredrik Elmgren, Baran Cürüklü, Jonathan Rodriguez, Joaquim Bastos, Marc Pinto, Intensity Normalization of Sidescan Sonar Imagery, the sixth International Conference on Image Processing Theory, Tools and Applications (IPTA'16), Finland, 2016 (accepted).

[7] C. de Moustier, "OS-CFAR detection of targets in the water column and on the seafloor with a multibeam echosounder," Oceans. San Diego, September 2013.

[8] Z. Jianhu, W. Xiao, Z. Hongmei, and W. Aixue. "A comprehensive bottom-tracking method for sidescan sonar image influenced by complicated measuring environment," IEEE Journal of Ocenic Engineeing, November 2016.

[8] Z. Jianhu, W. Xiao, Z. Hongmei, and W. Aixue. "A comprehensive bottom-tracking method for sidescan sonar image influenced by complicated measuring environment," IEEE Journal of Ocenic Engineeing, November 2016.

[9] V. Barnett and T. Lewis, Outliers in Statistical Data, Wiley Series in Probability and Mathematical Statistics; John Wiley & Sons; Chichester, 1994.